



## Article

# Biocompatible and Antimicrobial Cellulose Acetate-Collagen Films Containing MWCNTs Decorated with TiO<sub>2</sub> Nanoparticles for Potential Biomedical Applications

Madalina Elena David <sup>1,2,\*</sup> , Rodica Mariana Ion <sup>1,2</sup> , Ramona Marina Grigorescu <sup>1</sup> , Lorena Iancu <sup>1</sup>, Alina Maria Holban <sup>3</sup>, Florin Iordache <sup>4</sup> , Adrian Ionut Nicoara <sup>5</sup> , Elvira Alexandrescu <sup>1</sup>, Raluca Somoghi <sup>1</sup>, Sofia Teodorescu <sup>6</sup> and Anca Irina Gheboianu <sup>6</sup>

- <sup>1</sup> National Institute for Research and Development in Chemistry and Petrochemistry—ICECHIM, 060021 Bucharest, Romania; rodica\_ion2000@yahoo.co.uk (R.M.I.); rmgrigorescu@gmail.com (R.M.G.); lorena77ro@yahoo.com (L.I.); elvira.alexandrescu@icechim-pd.ro (E.A.); ralucaomoghi@outlook.com (R.S.)
- <sup>2</sup> Doctoral School of Materials Engineering Department, Valahia University of Targoviste, 130004 Targoviste, Romania
- <sup>3</sup> Faculty of Biology, University of Bucharest, 060101 Bucharest, Romania; alina\_m\_h@yahoo.com
- <sup>4</sup> Department of Biochemistry, Faculty of Veterinary Medicine, University of Agronomic Science and Veterinary Medicine, 011464 Bucharest, Romania; floriniordache84@yahoo.com
- <sup>5</sup> Faculty of Applied Chemistry and Materials Science, University Politehnica of Bucharest, 011061 Bucharest, Romania; adi.nicoara18@gmail.com
- <sup>6</sup> Institute of Multidisciplinary Research for Science and Technology, Valahia University of Targoviste, 130004 Targoviste, Romania; sofiateodorescu@yahoo.com (S.T.); anca@icstm.ro (A.I.G.)
- \* Correspondence: madalina.e.david@gmail.com



**Citation:** David, M.E.; Ion, R.M.; Grigorescu, R.M.; Iancu, L.; Holban, A.M.; Iordache, F.; Nicoara, A.I.; Alexandrescu, E.; Somoghi, R.; Teodorescu, S.; et al. Biocompatible and Antimicrobial Cellulose Acetate-Collagen Films Containing MWCNTs Decorated with TiO<sub>2</sub> Nanoparticles for Potential Biomedical Applications. *Nanomaterials* **2022**, *12*, 239. <https://doi.org/10.3390/nano12020239>

Academic Editors: Ana Maria Díez-Pascual and Ilaria Armentano

Received: 25 November 2021

Accepted: 10 January 2022

Published: 12 January 2022

**Publisher's Note:** MDPI stays neutral with regard to jurisdictional claims in published maps and institutional affiliations.



**Copyright:** © 2022 by the authors. Licensee MDPI, Basel, Switzerland. This article is an open access article distributed under the terms and conditions of the Creative Commons Attribution (CC BY) license (<https://creativecommons.org/licenses/by/4.0/>).

**Abstract:** This research focuses on the synthesis of multi-walled carbon nanotubes (MWCNTs) decorated with TiO<sub>2</sub> nanoparticles (NPs) and incorporated in cellulose acetate-collagen film in order to obtain a new biomaterial with potential biomedical applications and improved antimicrobial activity. The successful decoration of the MWCNTs with TiO<sub>2</sub> NPs was confirmed by several structural and morphological analysis, such as Fourier transformed infrared spectroscopy, Raman spectroscopy, X-ray diffraction and transmission electron microscopy. The obtained nanocomposites were further incorporated into cellulose acetate-collagen films, at different concentrations and absorption kinetics, antimicrobial activity and in vitro biocompatibility of the obtained films was investigated. The antimicrobial tests sustained that the presence of the nanocomposites into the polymeric matrix is an important aspect in increasing and maintaining the antimicrobial activity of the polymeric wound dressings over time. The biocompatibility and cytotoxicity of the obtained films was evaluated using cellular viability/proliferation assay and fluorescent microscopy which revealed the ability of the obtained materials as potential wound dressing biomaterial.

**Keywords:** wound dressing biomaterial; decorated carbon nanotubes; nanoparticles; antimicrobial properties

## 1. Introduction

In the past several years, medicine has faced real challenges regarding the bacterial spread, mostly because bacteria have evolved in order to survive antimicrobial medications by developing resistance mechanisms [1]. This issue continues to remain a major problem for hospitals and contribute significantly to the rate of morbidity, mortality and cost of care, that aggravates the problem mainly in developing countries where resources are scarce and staffs are always in short supply [2,3]. Nosocomial infections are common in burn patients due to the typical features of the disease: loss of the first line of defence against microbial invasion; avascularised tissue that offers a promising environment for microbial development; modifications in the specific and nonspecific constituents of the

immune system; and extended hospitalisation and therapeutic procedures [4,5]. Prolonged administration of antibiotics, often administered in combination, results in selection of multidrug resistant nosocomial strains which belong mainly to several bacterial species, such as Gram-positive (i.e., *Staphylococcus aureus*, *Streptococcus sp.*, *Micrococcus sp.*) and Gram-negative (i.e., *Escherichia coli*, *Pseudomonas aeruginosa*) bacteria, and sometimes yeasts (i.e., *Candida albicans*) [6–8].

Classical treatment of infections involves systemic antibiotic administration for long periods of time, that lead to difficulties due to its low specificity, low efficiency and/or increased selection of bacterial resistance [8]. Worldwide, poor wound healing affects many people, due to the poorly regulated features of the healthy tissue repair response. In order to avoid these complications, new antibacterial systems based on polymers and nanoparticles were investigated. The ideal wound dressing should provide protection against bacterial infection, promote angiogenesis, provide a moist environment and enhance epidermal migration [9,10]. Natural polymers are generally accepted for wound-healing applications because of their ideal properties, but most of them highlight limited or no antimicrobial activity [11]. Polysaccharides are natural biopolymers obtained from plant sources, with excellent biocompatibility [12]. An example belonging to this class is cellulose acetate (CA) which has been used for the biomaterials expansion of various biomedical and tissue engineering applications [13]. CA provides excellent biocompatibility, biodegradability, but the most important characteristic is that it has the potential to improve the cellular interaction between fibroblast cells and biomaterial [13–15]. These characteristics have made CA the right candidate for wound dressing applications. In recent years, researchers have mixed CA with the other polymers in order to obtain a biomaterial with enhanced properties for wound dressing applications. Collagen is the most common fibril protein in the human constitution, of about 30% of the total protein mass. This protein serves both a structural role being the basic protein of connective tissues in skin and bone, and a functional role being involved in complex mechanisms of tissue growth and repair [11]. This protein attracts attention because of its good biocompatibility, facile biodegradation (its degradation products being absorbed without inflammation), permeability and establishing strong interactions between the cells (due to stimulation of specific cell-morphology phenotypes) [11,15].

Nanomaterials are immersed in polymeric wound coverage matrices with the purpose to offer antibacterial activity, enhanced the angiogenic potential and cell proliferation and thus, assuring fast wound healing [16,17]. Recently, carbon nanotubes (CNTs) and decorated carbon nanotubes have attracted great attention as additive in biopolymers for the development of novel composite biomaterials, due to their antimicrobial activity, relatively high biocompatibility, promote angiogenesis, unique chemical and physical properties [18–20]. Pristine CNTs may induce some toxic reactions, but it has been demonstrated that the addition of polar functional groups to the CNTs surface considerably reduces their toxicity. The CNTs are capable to damage the cell membrane in microorganisms by direct contact, which results in bacterial cell death. The bacteriostatic properties of CNTs are assigned due to their high surface/volume ratio and large inner volume [21]. Laganà P. investigated the antimicrobial properties of MWCNTs, both pristine and functionalised, at two concentrations (50 and 100  $\mu\text{g}/\text{mL}^{-1}$ ), against bacterial strains isolated from hospital-acquired infections (*P. aeruginosa*, *K. Pneumoniae*, *E. coli* and *S. aureus*). It was reported that both types of MWCNTs and doses inhibited the bacterial strains and the functionalised MWCNTs exhibited a greater inhibiting effect, compared to pristine MWCNTs [22]. Moreover, it was demonstrated that the incorporation of a small concentration of MWCNTs (0.1%) in a polydimethylsiloxane (PDMS) matrix was able to reduce the *E. coli* adhesion with 20% [23]. When the concentration of MWCNTs was increased at 1% in the PDMS matrix a 60% reduction of *E. coli* adhesion was achieved [24]. In another study, it was demonstrated that *Staphylococcus sp.* did not grow on MWCNT composite films, suggesting that these films can inhibit microorganism attachment and biofilm formation on medical devices [25].

Presently, these nanotubes are being functionalised by different kinds of molecules or nanoparticles with the purpose of increasing drug delivery potential and improving their activity [26]. In the last years, MWCNTs have been successfully applied in the medical field, because CNTs exhibit better wound-healing properties comparing with other non-metallic nanomaterials, due to its property to promote cell migration when incorporated in hydrogels [27]. Ravanbakhsh H. and co-workers obtained an injectable hydrogel based on MWCNTs and glycol chitosan in order to investigate its potential on human dermal fibroblast cells (HDF). It was observed that small concentrations of CNT significantly increase cell migration in hydrogels, and accelerate tissue regeneration and wound healing in situations where there is insufficient migration in the unloaded matrix [20]. In another study, solubilised collagen Type I was used and polymerised in the presence of dispersed CNTs and HDF in order to obtain new biomaterials with HDF inserted directly in the matrix. After 7 days, it was reported that the viability of HDF was constantly increased, and the cell morphology was not perturbed by the existence of CNTs. Electrical conductivity of the constructs varied from 3 to 7 mS cm<sup>-1</sup>, depending on CNTs loading level, thus suggesting, that the electrical conductivity of cell-seeded collagen gels can be enhanced with the incorporation of CNTs [28]. Kittana N. and co-workers tested and compared the effect of chitosan complexed SWCNT and MWCNT hydrogels on 3T3 fibroblast cell line, in order to investigate the potential of these composites as wound-healing applications. The results sustained that the fibroblasts were viable in the presence of the complexes and were able to effectively organise and contract the extracellular matrix. Moreover, the composites were tested by in vivo on CC-72 line mice and it was observed that both types of complexes improved the re-epithelialisation of the wounds healing [26]. In another study, Murugesan B. and co-workers synthesised heteroatom (N, F, P/B)-incorporated MWCNTs by self-assembling ionic liquids in order to study their efficacy in wound healing. Their antibiofilm activity against *K. pneumoniae*, *P. aeruginosa*, *E. coli* and *B. subtilis* was investigated and the results revealed greater effectiveness for the obtained compositions, compared to pristine MWCNTs. Moreover, the synthesised materials were tested for its wound-healing ability in Wistar rats. It was reported that cells cultured on these materials displayed exceptional healing ability [29]. Das B. and co-workers studied the wound-healing potential of eco-friendly hyperbranched polyurethane and in situ prepared MWCNTs decorated with Fe<sub>3</sub>O<sub>4</sub> nanoparticles. It was reported that the obtained dressing patch presented excellent in vivo wound-healing potency in albino mice with an enhanced wound-closure rate [30].

The aim of this study is to design and characterise hybrid nanomaterials based on MWCNTs-TiO<sub>2</sub> incorporated in cellulose acetate-collagen film in order to obtain a potential wound dressings biomaterial with enhanced antimicrobial properties.

## 2. Materials and Methods

### 2.1. MWCNT-TiO<sub>2</sub> Synthesis

MWCNTs used in this study were obtained by chemical synthesis, purified and functionalised in our previously study [31] and the decoration of the MWCNTs with nanoparticles was performed more easily. Due to the fact that the nanotubes surface is inert, a chemical treatment is required in order to make it more active to react with other chemical compounds. The obtained MWCNTs were used as template and stabiliser for nanoparticles formation in order to obtain the nanotubes decoration. The in situ decoration of MWCNTs was carry out by dispersing 0.03 g nanotubes into 30 mL isopropanol (C<sub>3</sub>H<sub>8</sub>O, *p* > 99%, CHIMREACTIV, Bucharest, Romania), under sonication for 1 h. Subsequently, 3 wt% titanium (IV) isopropoxide (C<sub>12</sub>H<sub>28</sub>O<sub>4</sub>TiA, *p* > 98%, ACROS Organics, Geel, Belgium) in 20 mL isopropanol was added dropwise into the MWCNTs solution, under vigorous stirring. The obtained mixture was stirred for 2 h, at room temperature and then the solution was filtered, washed and dried at 100 °C, for 2 h. Finally, the product was sintered at 500 °C, for 30 min.

## 2.2. Biocomposite Materials Synthesis

4% cellulose acetate (Fluka, Buchs, Switzerland) and 4% collagen from bovine (Sigma-Aldrich, Schnellendorf, Germany) were separately dissolved in 100 mL glacial acetic acid and water (70 mL and 30 mL, respectively) and stirred for 3 h. After the solutions have completely dissolved, the collagen solution was added into the cellulose acetate solution and stirred for 30 min. Then, 50 mL from the stock solution was cast in Petri dishes, in order to obtain cellulose acetate-collagen (CC) films. Moreover, 50 mL of the stock solution was mixed for 30 min with 0.01 g, 0.025 g and 0.05 g of MWCNT\_TiO<sub>2</sub>, in order to obtain MWCNT\_TiO<sub>2</sub>@CC films (according to Table 1). Samples were placed into Petri dishes, crosslinked with 1% glutaraldehyde (Merck, Darmstadt, Germany) by spraying and kept at room temperature for 48 h in order to evaporate the solvent.

**Table 1.** Optimisation of films.

Sample No.	Sample Coding	Ratio of Cellulose Acetate/Collagen (g/g)	Observation
1	CC	1:1	-
2	CC@MWCNT_TiO <sub>2</sub> 0.01	1:1	0.01 g of MWCNT_TiO <sub>2</sub> was added over the solution
3	CC@MWCNT_TiO <sub>2</sub> 0.025	1:1	0.025 g of MWCNT_TiO <sub>2</sub> was added over the solution
4	CC@MWCNT_TiO <sub>2</sub> 0.05	1:1	0.05 g of MWCNT_TiO <sub>2</sub> was added over the solution

## 2.3. Structural and Morphological Analyses

### 2.3.1. Fourier Transformed Infrared Spectroscopy (ATR-FTIR)

ATR-FTIR was registered with a GX-type FTIR spectrometer (Perkin Elmer, Waltham, MA, USA), in the 4000–400 cm<sup>-1</sup> range, 4 cm<sup>-1</sup> resolution, by accumulating and mediating 32 spectra.

### 2.3.2. Raman Spectroscopy Analysis

Raman spectroscopy was achieved with a Horiba equipment (Labram HR Evolution, Pailaiseau, France) having a 514 nm excitation wavelength and a 50× objective with a 10 s acquisition time.

### 2.3.3. X-ray Diffraction Analysis (XRD)

A Rigaku Ultima IV diffractometer (Rigaku, Tokyo, Japan) using Cu K α radiation ( $\lambda = 1.54 \text{ \AA}$ ), 40 kV accelerating voltage of the generator radiation and 30 mA emission current was used in order to obtain the XRD diffractograms. The diffractograms were recorded in parallel beam geometry over  $2\theta = 10^\circ$  to  $90^\circ$  continuously at a scan rate of  $4^\circ/\text{min}$ .

### 2.3.4. Transmission Electron Microscopy (TEM)

TEM analysis was performed by using a G2 F20 TWIN Cryo-TEM (Philips, Eindhoven, The Netherlands) with 200 keV accelerating voltage. Initially, the obtained samples were pre dispersed in distilled water and sonicated for one hour. For microscopy examination, one drop of the aqueous dispersion was placed on the holey formvar grid.

### 2.3.5. Scanning Electron Microscopy (SEM)

The films morphology was investigated using an FEI Quanta Inspect FEG Scanning Electron Microscope (FEI, Hillsboro, OR, USA) with 30 kV accelerating voltage. The obtained films were previously sputtered with gold for 30 s.

#### 2.4. Absorption Kinetics

Absorption kinetics of a film is an important parameter in tissue engineering, in order to confirm the stability of porous wound-dressings. This method offers evidence on how the film will act in contact with the body fluids and also, about their interaction that can limit the process of cellular differentiation [8]. In this study, the simulated body fluid (SBF) solution was obtained, according to the Kokubo's methodology [32].

Each sample was cut into a cylinder of 3 cm diameter, weighed (initial mass,  $W_i$ ) and completely immersed in 20 mL SBF, at a temperature of 37° C for various periods of time. At specified time, the samples were taken off, the excess fluid from their surface was removed and weighed (mass at time  $t$ ,  $W_t$ ). Absorption ratio was calculated according to Equation (1):

$$\text{Absorption ratio \%} = \frac{W_t - W_i}{W_i} \quad (1)$$

#### 2.5. Hardness Measurements

A Shore hardness durometer, model PosiTector SHD-A, DeFelsko, Ogdensburg, NY, USA was used in order to investigate the hardness of the obtained films. Ten measurements were recorded for each film and average value was calculated.

#### 2.6. Antimicrobial Analysis

##### 2.6.1. Microbial Strains and Growth Conditions

*S. aureus* ATCC 25923, *E. coli* ATCC 25922 and *C. albicans* ATCC 10231, were obtained from American Type Culture Collection (ATCC, Manassas, VA, USA), and used in order to investigate the antimicrobial activity of the obtained biofilms. In order to obtain a fresh culture used for the subsequent studies, glycerol stocks were streaked on LB agar (for bacteria) or Sabouraud agar (for *C. albicans*). All experiments were implemented in triplicate.

##### 2.6.2. Qualitative Antimicrobial Assay—Growth Inhibition

An adapted diffusion test, with regard to the general rules exposed in the CLSI 2020 was used in order to qualitatively monitor the antibacterial activity of the obtained films.

Initially, a 0.5 McFarland bacterial suspension ( $1.5 \times 10^8$  CFU/mL) was obtained in sterile saline (0.9% NaCl solution) and used as a standardised inoculum to swab inoculate Petri dishes containing nutritive agar. The films were cut (6 mm diameter) and sterilised by UV exposure for 30 min before use. The cut films were aseptically placed on the inoculated Petri dishes and incubated (37 °C for 20 h). After incubation, the diameter of growth inhibition developed around each film was measured and noted (in mm).

##### 2.6.3. Monospecific Biofilm Development

The antibiofilm performance was carried out by transferring the obtained films (6 mm in diameter, sterile) in sterile 24-well plates with 1 mL nutritive broth and inoculation of 10 µL of bacterial suspension of 0.5 McFarland standard density. Then, the as prepared plates were incubated (37 °C for 24 h). After that, the films were gently washed with 1 mL of sterile saline solution and then, the samples were transferred in 1.5 mL centrifuge tubes, in 1000 µL sterile saline solution, followed by vortexing the obtained films, for 30 s in order to ensure the detachment of biofilm cells in suspension. In order to evaluate the viable colony formation (CFU/mL), serial 10-fold dilutions were obtained and then inoculated on nutrient agar.

##### 2.6.4. Evaluation of the Planktonic Development of Microorganisms

Planktonic development in the company of the obtained films was studied in nutritive broth. Films of 6 mm in diameter were positioned in sterile 24-well plates and 1 mL of nutritive broth and 10 µL of the previously obtained 0.5 McFarland bacterial suspensions in PBS were added. Specimens were incubated at 37 °C for 24 h. The obtained bacte-

rial culture (150  $\mu\text{L}$ ) was relocated to 96-well plates and the absorbance at 600 nm was spectrophotometrically investigated, in order to determine the development of planktonic (free-floating) cultures.

### 2.7. Statistical Analysis

Biological results were studied by the one-way ANOVA repeated measures test. The statistical analyses were achieved using GraphPad Prism Software, v. 9.2. The obtained results were compared by Tukey's test ( $p < 0.05$ ).

### 2.8. Cellular Viability Assays

#### 2.8.1. MTT Assay

MTT [3-(4,5-dimethylthiazolyl)-2,5-diphenyltetrazolium bromide] test (Vybrant<sup>®</sup> MTT Cell Proliferation Assay Kit, Thermo Fischer Scientific, Waltham, MA, USA) was used in order to investigate the biocompatibility of the obtained films. Human dermal fibroblast HDFn cells (ATCC, PCS-201-010, Manassas, VA, USA) were developed in DMEM medium (Sigma-Aldrich, Saint Luis, MO, USA) and supplemented with 10% foetal bovine serum, 1% antibiotics (penicillin and streptomycin) (Sigma-Aldrich, Saint Luis, MO, USA), changed twice a week. The HDFn cells were grown in 96-well plates, with a seeding density of 3000 cells/well in the presence of films, for 72 h. Then, 15 mL (12 mM) of MTT was added to the cells and incubated at 37 °C for 4 h. A solution of 1 mg sodium dodecyl sulphate in 10 mL HCl (0.01 M) was added and pipetted vigorously to solubilise the formed formazan crystals. A TECAN Infinite M200 spectrophotometer (Männedorf, Switzerland) was used to evaluate the optical density of the solubilised formazan, at 570 nm, after 1 h.

#### 2.8.2. Fluorescence Microscopy

In order to evaluate the biocompatibility of the obtained films a RED CMTPX fluorophore (Thermo Fischer Scientific, Waltham, MA, USA) was used. The CMTPX was added to the HDFn cell culture, in the presence of the obtained films. After 5 days, the viability and morphology of the HDFn were evaluated. The CMTPX fluorophore, at a concentration of 5  $\mu\text{M}$  and incubated for 30 min, was added in the culture medium with the purpose to permit the dye penetration into the cells. Lastly, the HDFn cells were washed with PBS. An Olympus CKX 41 digital camera driven by CellSense Entry software (Olympus, Tokyo, Japan) was used to visualise the cells.

## 3. Results and Discussions

### 3.1. Characterisation of MWCNT\_TiO<sub>2</sub>

The first stage of the research implies the characterisation of the MWCNT\_TiO<sub>2</sub> with the purpose of demonstrating the successful decoration of the nanotubes.

#### 3.1.1. FTIR Spectroscopy

FTIR spectra of MWCNTs\_TiO<sub>2</sub> confirms the presence of two important peaks, corresponding to C=C at 1632  $\text{cm}^{-1}$  (carbon nanotubes' skeleton) and Ti–O bonds at 419  $\text{cm}^{-1}$ , Figure 1. Moreover, the carbonyl group was confirmed by the peak at 1128  $\text{cm}^{-1}$  corresponding to the C–O stretching. A broad absorption can be observed at approximately 3400  $\text{cm}^{-1}$ , probably due to water presence.

#### 3.1.2. Raman Analysis

The Raman spectrum of MWCNT\_TiO<sub>2</sub> presented in Figure 2, confirms the specific band of anatase TiO<sub>2</sub>, such as 148.22  $\text{cm}^{-1}$ , 398.92  $\text{cm}^{-1}$ , 518.15  $\text{cm}^{-1}$  and 639.31  $\text{cm}^{-1}$ . Moreover, the specific bands of MWCNTs are present, at 1597.63  $\text{cm}^{-1}$  (G band), which refers to the crystalline nature of the MWCNTs and the band at 1346.29  $\text{cm}^{-1}$  (D band), which indicates the distortions on the MWCNTs surface. The presence of D and G bands confirms the interfacial interaction between MWCNTs and TiO<sub>2</sub> nanoparticles [33]. The ID/IG band ratio was calculated to be 0.842. Compared with the ID/IG band ratio of pure

MWCNTs (0.839) [18], it can be suggested that the increasing of the ID/IG band ratio occurs because of the structural defects in the carbon wall, confirming thus, the modification of the outer layers of the MWCNTs by nanoparticles deposition.

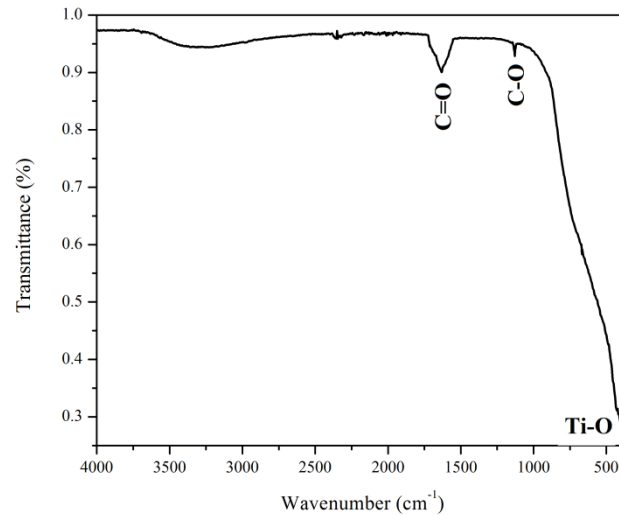


**Figure 1.** FTIR spectra of MWCNTs\_TiO<sub>2</sub>.

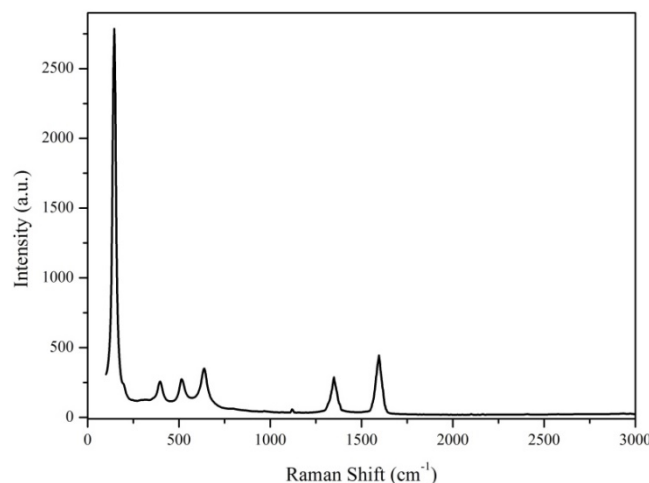


**Figure 2.** Raman spectra of MWCNTs\_TiO<sub>2</sub>.

### 3.1.3. XRD Analysis

The XRD pattern of the MWCNTs\_TiO<sub>2</sub> (Figure 3) confirms the presence of the diffraction peaks corresponding to MWCNTs structure (at 25.26° and 42.88°). The characteristic diffraction peaks of TiO<sub>2</sub> nanostructure observed at 37.99, 47.97, 54.54, 70.26, 75.04 and 82.71 are perfectly assigned to the crystal planes (110), (200), (211), (021) and (220) which confirm the anatase phase [34,35]. The peak at 25.26° corresponds to the crystal plane (002) reflection of MWCNTs and overlaps the crystal plane (101) reflection of anatase TiO<sub>2</sub>, peak that appears at 25.53°, confirming, thus, that the anatase phase was the major crystal in MWCNT/TiO<sub>2</sub> nanocomposites.

Scherrer's Equation (2) was used in order to calculate the crystallite size (*L*) of the MWCNTs\_TiO<sub>2</sub>. Table 2 shows the crystallite size of the nanomaterials.

$$L = K\lambda / \beta \cos \theta \quad (2)$$

where, *K* is Scherrer constant (0.91),  $\lambda$  is the X-ray wavelength (1.5406 Å),  $\beta$  is the full-width at half maximum and  $\theta$  is the Bragg angle (rad).

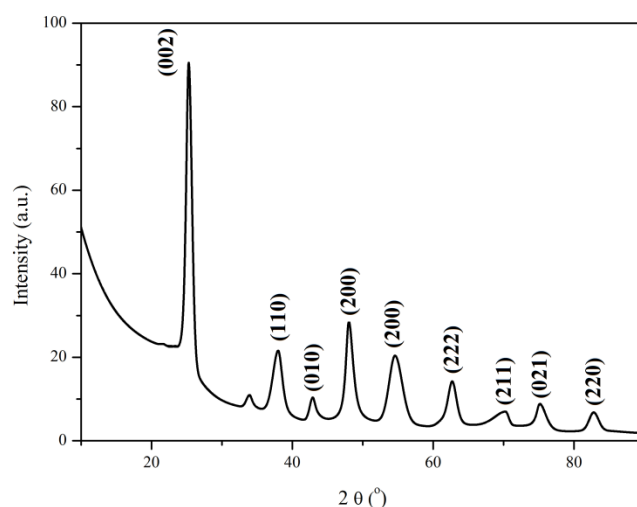


**Figure 3.** XRD pattern of MWCNTs\_TiO<sub>2</sub>.

**Table 2.** Summary of the XRD characterisation of synthesised MWCNTs and MWCNTs\_TiO<sub>2</sub>.

Sample	2θ (°)	2θ (rad)	β (°)	L (Å)	L (nm)
MWCNTs [18]	25.53	0.4456	4.08	20.18	2.018
MWCNTs_TiO <sub>2</sub>	25.267	0.2204	0.964	85.39	8.539

The significantly increased crystallite size in the case of MWCNTs\_TiO<sub>2</sub>, compared to pure MWCNTs could be explained by the higher size of the TiO<sub>2</sub> nanoparticles that covered the surface of the nanotubes (Table 2). MWCNTs\_TiO<sub>2</sub> shows the lowest distribution, that means largest crystallite size and lowest lattice strains [36]. The peak of decorated carbon nanotubes is four times narrower than MWCNTs indicating improved crystallinity that can impart higher mechanical properties in the nanocomposites.

### 3.1.4. TEM Analysis

The nanotubes synthesised in our previous work [31] have a wide size distribution, with a diameter of 10–50 nm and approximately 600 nm in length, confirming thus, that the obtained MWCNTs were shorts. The synthesised nanotubes presented only a few defects on their surface, which suggests that nanotubes are composed of quality graphite layers. In Figure 4, the obtained MWCNTs\_TiO<sub>2</sub> are presented. The TiO<sub>2</sub> NPs are successfully deposited on the surface of the nanotubes. The deposited nanoparticles have spherical shapes, with a diameter of about 15 nm. It can be observed that the nanoparticles are more intensely aggregated in some areas on the nanotubes surface.

## 3.2. Characterisation and Investigation of MWCNT\_TiO<sub>2</sub>@CC Films

The second stage of the research implies the characterisation of the CC film and MWCNT\_TiO<sub>2</sub> incorporated in CC films (MWCNT\_TiO<sub>2</sub>@CC) in order to investigate the potential of the films as wound dressing biomaterial. The obtained films presented a thickness of 0.148 mm (by calculating the arithmetic mean of 10 values).

### 3.2.1. FTIR Spectroscopy

The infrared spectrum of the obtained films is presented in Figure 5. The FTIR spectra of CC film demonstrate the existence of carbonyl group from the collagen, and the triple helix structure of collagen at 1638 cm<sup>-1</sup>—amide I, 1546 cm<sup>-1</sup>—amide II and at 1220 cm<sup>-1</sup>—amide III, from the N–H stretching of the hydrogen-bonded amide groups [13]. The presence of celluloses acetate is confirmed by its characteristic bands, such as the carbonyl vibration in the acetate substituent at 1730 cm<sup>-1</sup>, and the hydrogen oxygen vibration in hydroxyls or water presence at 3294 cm<sup>-1</sup>. The peak at 1359 corresponds to CH<sub>3</sub> groups



of the acetyl moiety and the peak at  $1022\text{ cm}^{-1}$  matches to ether (C–O–C) bonds of the glycosidic bond [37].

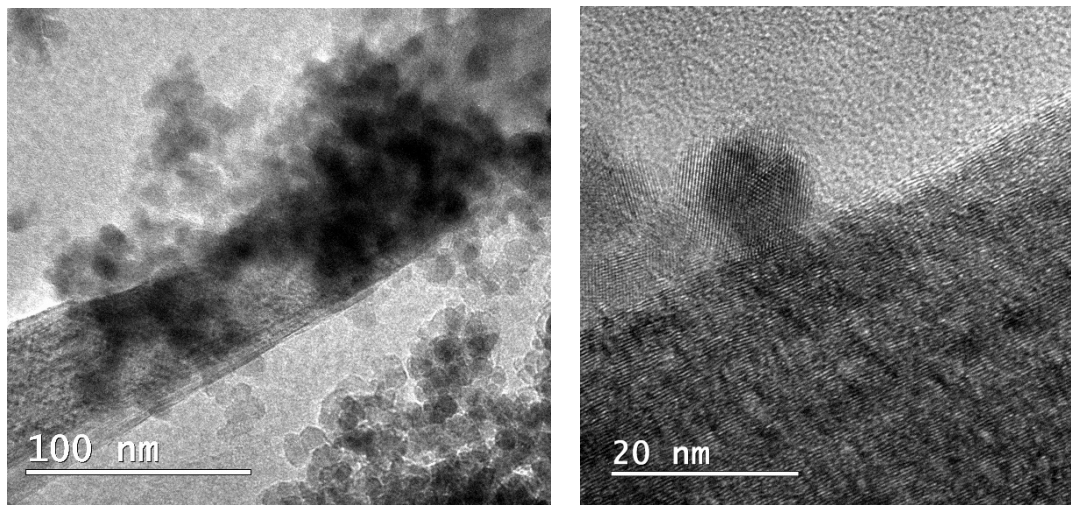


**Figure 4.** TEM micrographs of the obtained nanocomposites.

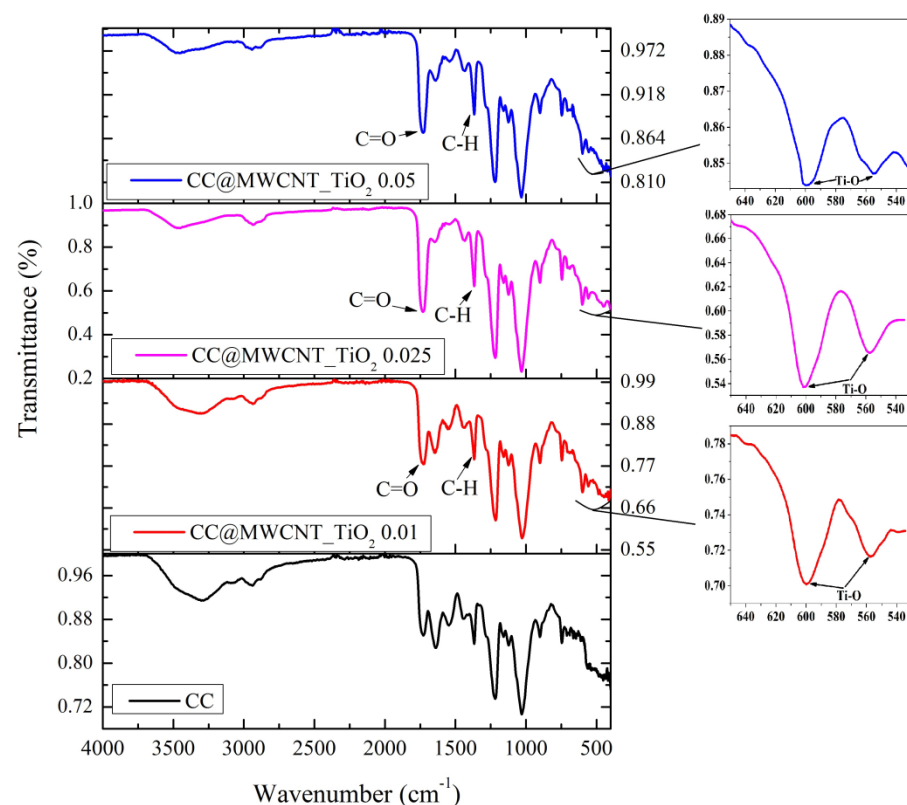


**Figure 5.** FTIR spectra of the obtained films.

By adding MWCNTs\_TiO<sub>2</sub>, new characteristic peaks are observed, especially when the nanocomposite concentration increased. The FTIR spectra shows sharper peaks at  $1371\text{ cm}^{-1}$  that are related to the C–H bonds characteristic of carbon nanotubes' skeleton and  $1730\text{ cm}^{-1}$  related to C=O from MWCNTs oxidation (indicating that carboxylic groups are formed due to the oxidation of some carbon atoms on the surface of the MWCNTs) [18,38]. The presence of TiO<sub>2</sub> nanoparticles was confirmed by the band at low wavenumber around  $605$  and  $558\text{ cm}^{-1}$ .

### 3.2.2. SEM Analysis

SEM micrographs of the obtained films are presented in Figure 6. Figure 6a,b illustrates the porous structure of the control sample (collagen and cellulose acetate without the antimicrobial agent). The porous film has mainly pore sizes of approximately 30 to 50  $\mu\text{m}$  in diameter and smaller pores of approximately 5–10  $\mu\text{m}$ . An open and interconnected relatively homogeneous porous structure can be observed for all the obtained films. When the antimicrobial agent was incorporated, a slight reduction of the pores dimensions was observed, mostly when the quantity of the agent increased. In all the cases, relatively homogeneous distribution of the agent can be observed. For the samples with increased concentration of nanocomposites, larger MWCNTs-TiO<sub>2</sub> aggregates are presented (between 1.5–3  $\mu\text{m}$  for CC@MWCNT-TiO<sub>2</sub> 0.01 film; to 5–30  $\mu\text{m}$  for CC@MWCNT-TiO<sub>2</sub> 0.05 film).

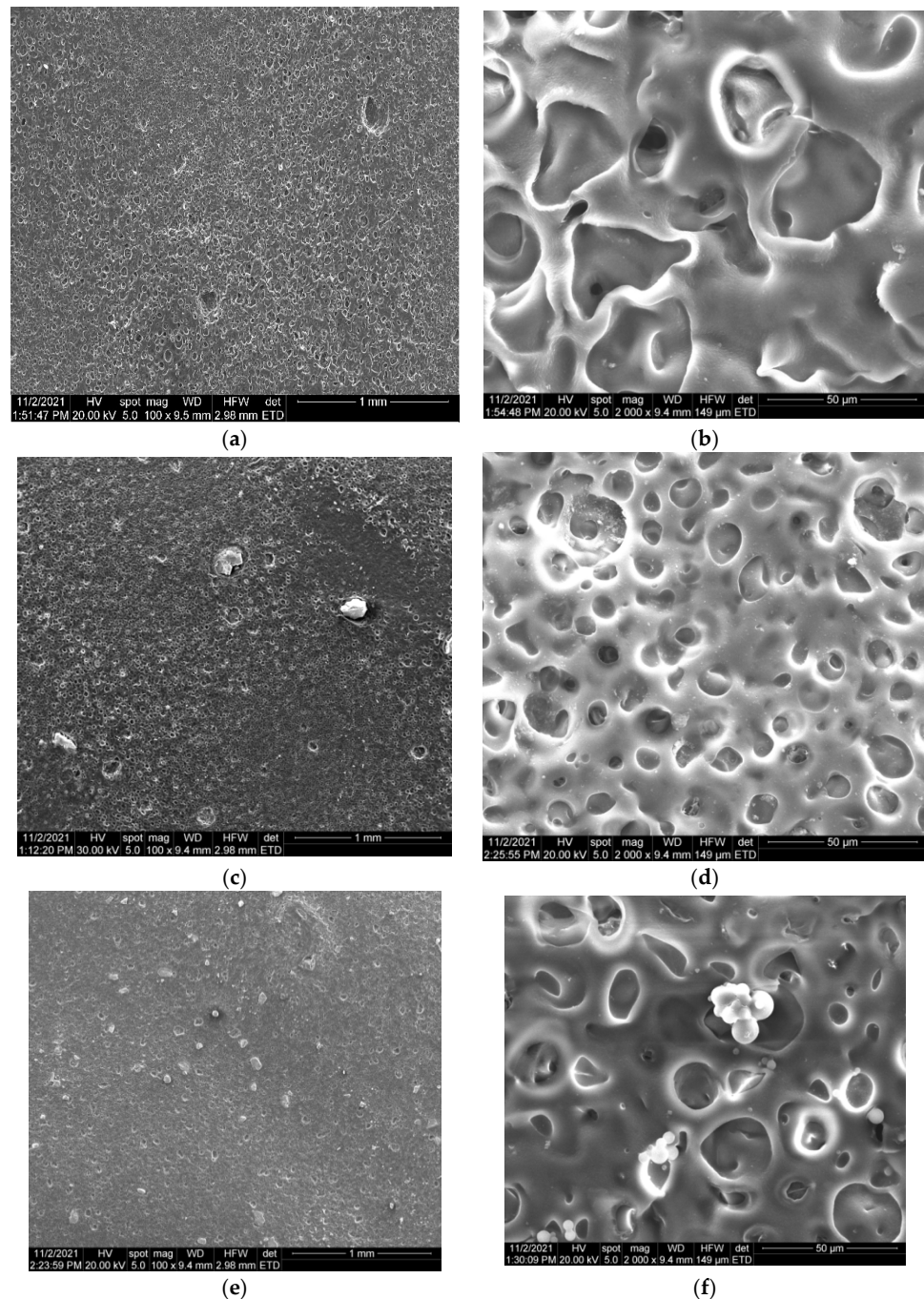
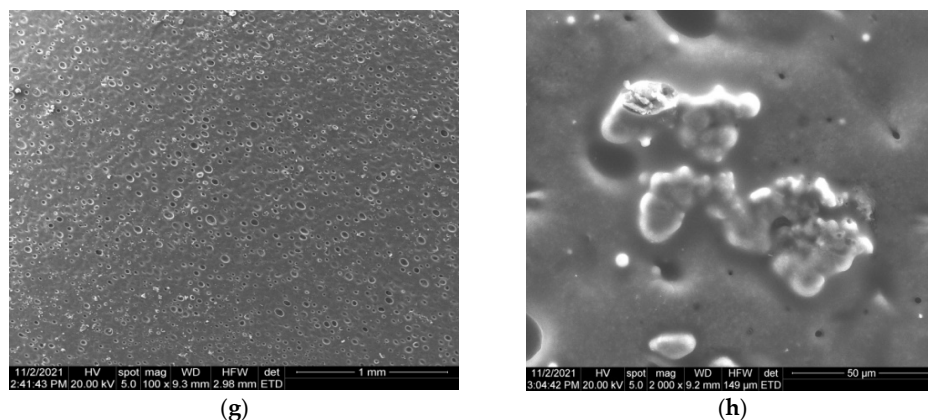


Figure 6. Cont.



**Figure 6.** SEM micrographs showing the morphology of the films: CC (a,b), CC@MWCNT\_TiO<sub>2</sub> 0.01 (c,d), CC@MWCNT\_TiO<sub>2</sub> 0.025 (e,f) and CC@MWCNT\_TiO<sub>2</sub> 0.05 (g,h).

### 3.2.3. Absorption Kinetics

In Figure 7 are presented the absorption kinetics for the obtained films. It can be seen that the absorption kinetics of the films decrease with increase in the amount of MWCNTs\_TiO<sub>2</sub>. This is attributed to the network structure formed between the nanomaterials and polymers, which prevent the absorption of a large quantity of water molecules. It can be observed that in the case of CC film, the maximum absorption of about 66% was reached after 60 min, while when the nanomaterials were incorporated lower absorption maxima can be observed. In the case of CC film, a slight decrease in absorption which stabilises after 300 min can be observed and also, this tendency is observed for the film with the lowest content of MWCNTs\_TiO<sub>2</sub> (0.01 g). When the nanocomposite content increased, lower maximum absorptions are observed, and absorption kinetics has a decreasing tendency over time.

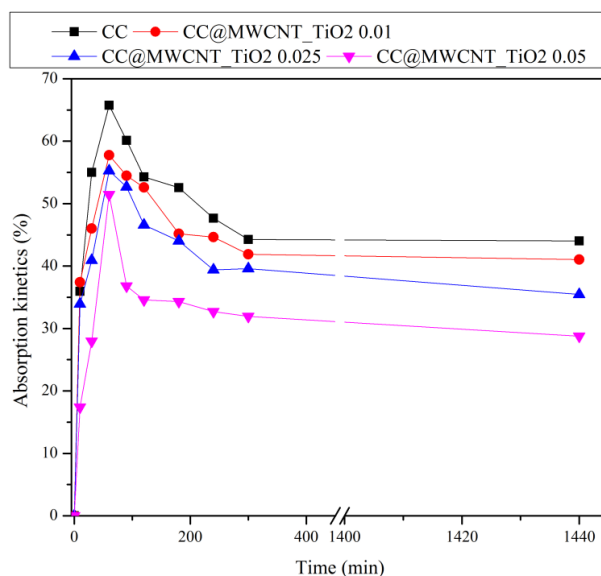


**Figure 7.** Absorption kinetics of the obtained films.

### 3.2.4. Hardness

Maintaining a good mechanical character of the material is a very important feature of dressing. It has been reported in several studies that the incorporation of NPs into polymer composites significantly changes their mechanical properties [39]. Thus, the hardness of the obtained films was measured. As can be observed in Figure 8, the behaviour suggests

that the bonding and microstructure of the films change significantly with increasing the MWCNTs\_TiO<sub>2</sub> content. It can be observed that even when a low content of MWCNTs\_TiO<sub>2</sub> was incorporated into the CC solution, effective hardness was obtained, compared to CC film. The large surface area of the nanomaterials leads to a stronger interfacial interaction between them and polymer molecules, and stress is better transferred through the materials which are subjected to mechanical effort, resulting in better properties of the CC films. Therefore, incorporating MWCNTs\_TiO<sub>2</sub> as reinforcing elements into the film could result in additional strength to the composite biomaterials.

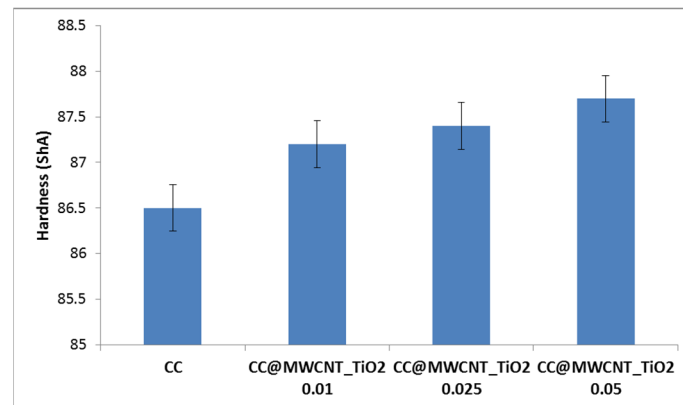


Figure 8. Hardness of the obtained films.

### 3.2.5. Antimicrobial Analysis

#### Qualitative Antimicrobial Assay—Growth Inhibition

The obtained results demonstrated that the films presented a different antibacterial activity, depending both on the tested strain and the MWCNTs\_TiO<sub>2</sub> content (Figure 9). As can be observed, the highest values of growth inhibition zones were obtained for the film with the highest MWCNTs\_TiO<sub>2</sub> content. The largest area of inhibition was obtained for *E. coli*, this can be related with the sensitivity of bacteria to nanocomposites that differs according to the interface provided by the bacterial membrane. It is well-known that Gram-positive bacteria are less sensitive to nanomaterials, compared to Gram-negative bacteria, because of their thicker peptidoglycan layer [40].

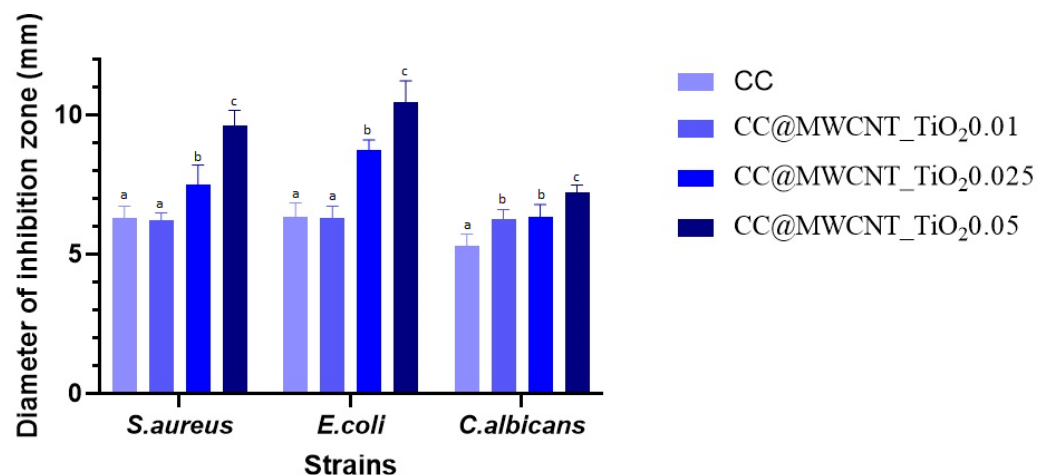
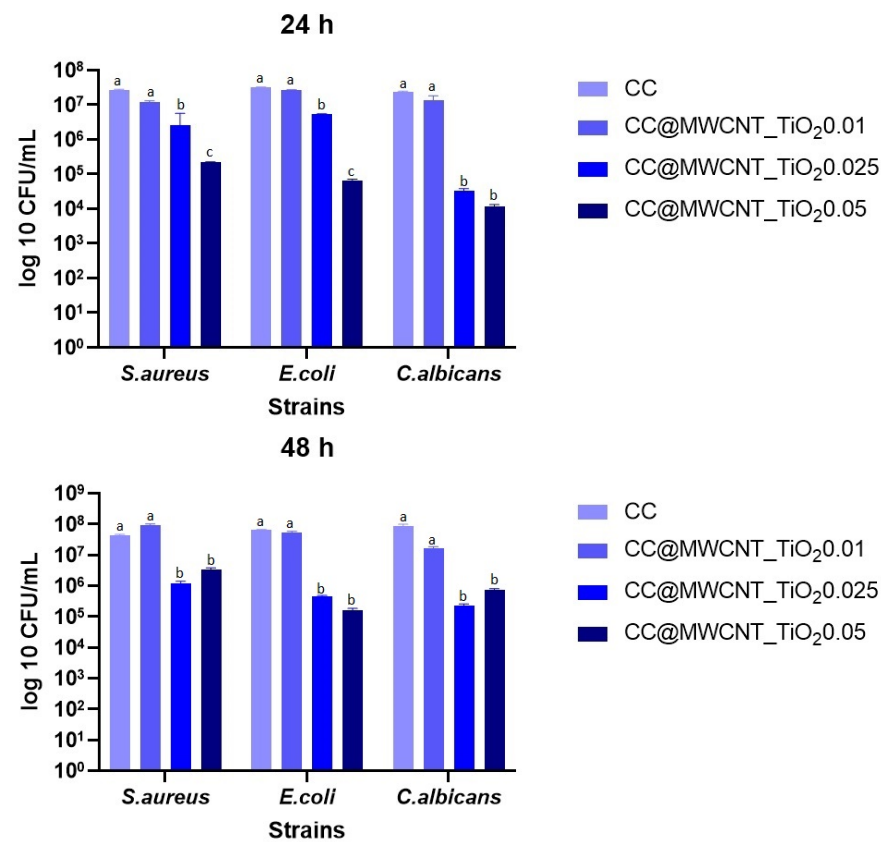


Figure 9. Graphic representation of growth inhibition diameters (mm) obtained after the cultivation of evaluated bacterial strains in the presence of films. Different small letters (a, b and c) indicate statistically significant differences between films ( $p < 0.05$ ).

### Monospecific Biofilm Development

The obtained results sustain that the biofilm expansion was significantly reduced at 24 h in all the cases of tested strains, when the films with the highest concentrations of nanocomposites were used (CC@MWCNTs\_TiO<sub>2</sub> 0.025 and CC@MWCNTs\_TiO<sub>2</sub> 0.05), so we can suggest that biofilm inhibition is dependent on the nanocomposites concentration (Figure 10). This tendency is maintained after 48 h, which suggests that the films are capable to offer protection over time. These results demonstrate that the presence of the hybrid nanomaterials is an important point. Many studies demonstrated the antimicrobial character of TiO<sub>2</sub> NPs [41,42] and MWCNTs [18,43]. These data suggest that the films can combat specific pathogens, especially in wound-healing application, due to their higher effectiveness against Gram-positive and Gram-negative bacteria and yeast.



**Figure 10.** Values of log<sub>10</sub> CFU/mL for the tested bacterial strains, expressing biofilm-embedded cells developed on the obtained films after 24 h (**up**) and 48 h (**bottom**) incubation. Different small letters (a, b and c) indicate statistically significant differences between films ( $p < 0.05$ ).

### Evaluation of the Planktonic Development of Microorganisms

Planktonic development inhibition results showed growth inhibition in cases of *S. aureus* and *E. coli* when the nanocomposites are present, even at the lowest concentration. Figure 11 shows that the highest bacterial growth inhibition occurs for the film containing the highest amount of MWCNTs\_TiO<sub>2</sub>. After 48 h, this tendency is maintained indicating that the antibacterial nanocomposites from the polymeric matrix could be released affecting the evolution of bacterial cells (Figure 11 bottom).

#### 3.2.6. Cellular Viability/Proliferation Assay (MTT Assay) and Fluorescence Microscopy

MTT assay presented in Figure 12 shows that the obtained films present absorbance values close to the control sample at 24 h to 72 h, proving their non-toxicological effect. The metabolic activity of HDFn in the presence of films demonstrates to be higher than in

the control cells, suggesting that cells are viable, improving thus the proliferation capacity. At 72 h, an increased proliferation capacity was observed for the films containing low and moderate quantity of nanocomposites (0.01 and 0.025 g MWCNTs\_TiO<sub>2</sub>), compared to the control. These results sustain that the nanocomposites dose is one of the main factors in the relationships between the responding cell type and nanomaterials. An ideal biomaterial-based nanoparticles has to present the ability to minimise cytotoxicity to a range of potentially exposed cells. Regarding this, there are several reports that sustain that TiO<sub>2</sub> nanoparticles and MWCNTs are non-toxic, and their exposure does not lead to membrane damage or cell death [44–46].

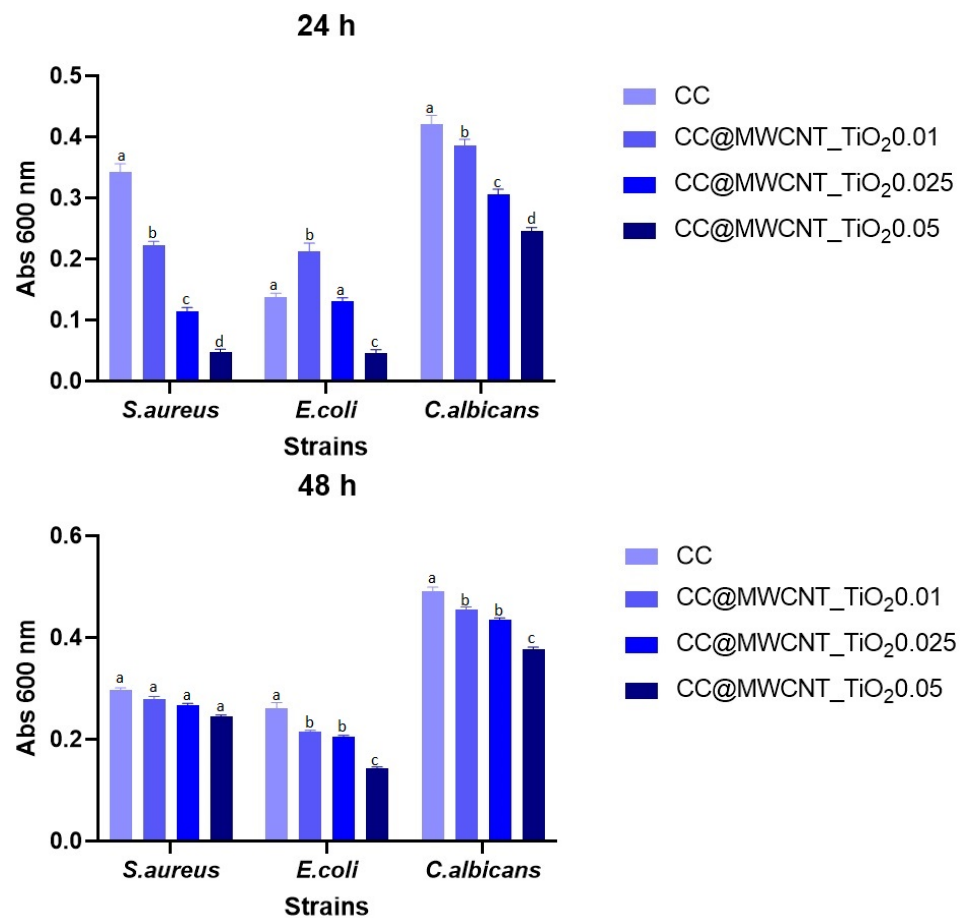


**Figure 11.** Absorbance at 600 nm indicating growth of planktonic cultures in the presence of films at 24 h (**up**) and 48 h (**bottom**) at 37 °C. Different small letters (a, b and c) indicate statistically significant differences between films ( $p < 0.05$ ).

Fluorescence microscopy images show that HDFn cells are viable, and the films have no cytotoxic effect, approving the biochemical assay. By fluorescence microscopy images it can be observed that the cellular metabolism of the cells is active, due to the fact that cells absorb the fluorophore CMTPX dye in the cytoplasm, demonstrating their viability after five days of incubation with HDFn cells. In Figure 13b no dead cells or cell fragments are detected when the cells are in contact with the film; the HDFn presents a normal morphology, with a normal fibroblast phenotype that preserves their initial morphology, with homogenous sizes and density distributions in the culture well plates. All the samples present extensions that demonstrate that the phenotype is active. In Figure 13d,e, HDFn is more abundant and has more elongated extensions suggesting that these materials stimulated the cells. This occurs because of the activity of the cytoskeleton and principally represents actin filaments and microtubules. As the HDFn cells are involved in several cellular processes, such as cell migration and wound healing, it can be concluded that the

seeded cells demonstrated a good bioactivity for the studied films, especially when the concentration of MWCNTs\_TiO<sub>2</sub> increased.

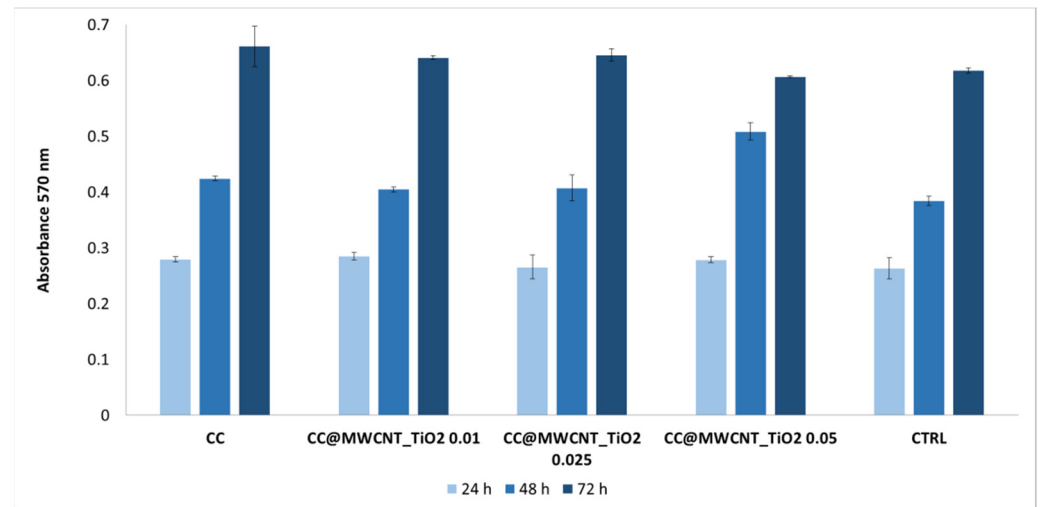


**Figure 12.** The viability of HDFn cells in the presence of films by MTT assay; the results are presented as the mean  $\pm$ S.D. of three replicates.

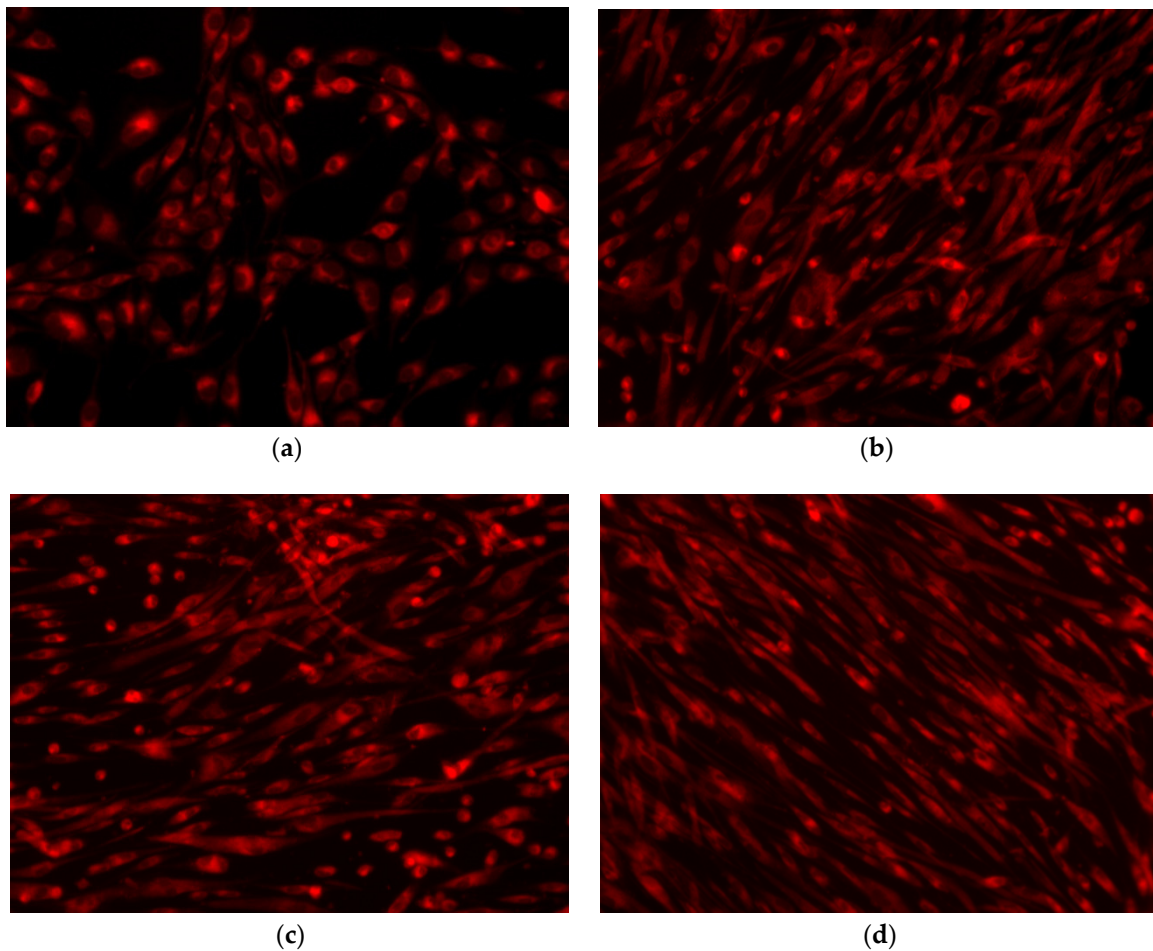


**Figure 13.** *Cont.*

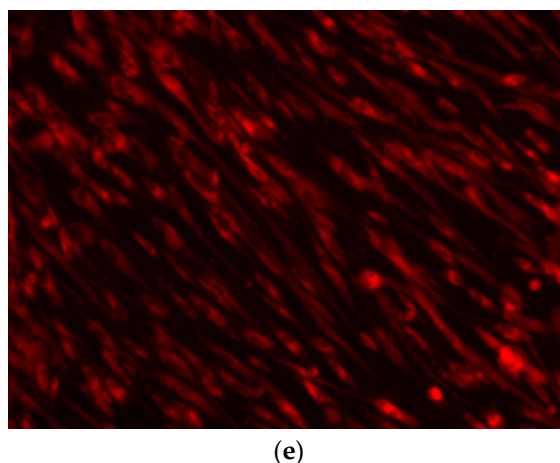


**Figure 13.** Fluorescence images showing the viability of HDFn cells coloured with CMTPIX fluorophore: (a) control sample; (b) CC; (c) CC@MWCNT\_TiO<sub>2</sub> 0.01; (d) CC@MWCNT\_TiO<sub>2</sub> 0.025 and (e) CC@MWCNT\_TiO<sub>2</sub> 0.05 film.

#### 4. Conclusions

In this study, we reported obtaining nanocomposites based on decorated MWCNTs with TiO<sub>2</sub> NPs incorporated in cellulose acetate-collagen film in order to test their potential as antimicrobial wound dressing biomaterial. The decoration was confirmed by structural and morphological analyses, such as Fourier transformed infrared spectroscopy, Raman spectroscopy, X-ray diffraction and transmission electron microscopy. The attached nanoparticles on the nanotubes surface presented spherical shapes with diameter of about 15 nm. By TEM analysis it was observed that the nanoparticles are aggregated to the MWCNTs surface.

After obtaining the nanocomposites, they were incorporated in cellulose acetate-collagen film. The porous nature of the obtained biomaterials was established through SEM analysis, highlighting the micrometric pores, with homogenous distribution of TiO<sub>2</sub> NPs into the polymeric matrix. The films absorbed a lower quantity of SBF when the MWCNTs\_TiO<sub>2</sub> quantity increased as demonstrated by absorption kinetics. This is attributed to the network structure formed between the nanomaterials and polymers, which prevents the absorption of large quantity of water molecules. The antimicrobial tests sustained that the presence of the nanocomposite in the polymeric matrix plays a key role in increasing and maintaining the antimicrobial activity of the polymeric wound dressings, over time. Moreover, the highest antimicrobial activity was obtained for the films with the highest concentrations of nanocomposites (CC@MWCNTs\_TiO<sub>2</sub> 0.025 and CC@MWCNTs\_TiO<sub>2</sub> 0.05). Overall, these films strongly inhibited the growth of both Gram-positive and Gram-negative strains, improving the cell proliferation capacity. Our results support the idea that the obtained films containing MWCNTs\_TiO<sub>2</sub> are biocompatible and possess antimicrobial activity, becoming thus successful candidates for the development of competent and efficient wound dressings. Further, *in vivo* studies will be designed to show the full range of bioactivity in our next paper.

**Author Contributions:** Conceptualisation, M.E.D.; methodology, M.E.D.; validation, R.M.I.; formal analysis, M.E.D.; investigation, A.M.H., F.I., A.I.N., E.A., R.S., S.T., A.I.G. and M.E.D.; data curation, M.E.D.; writing—original draft preparation, M.E.D.; writing—review and editing, R.M.I., R.M.G. and L.I.; supervision, R.M.I.; funding acquisition, R.M.I. All authors have read and agreed to the published version of the manuscript.

**Funding:** This work was supported by a grant of the Romanian Ministry of Research and Innovation, CCCDI—UEFISCDI, project number PNIII-P1-1.2-PCCDI-2017-0476/51PCCDI/2018, within PNCDI III.

**Data Availability Statement:** Data is contained within the article.



**Conflicts of Interest:** The authors declare no conflict of interest.

## References

1. Coates, A.; Hu, Y.; Bax, R.; Page, C. The future challenges facing the development of new antimicrobial drugs. *Nat. Rev. Drug Discov.* **2002**, *1*, 895–910. [\[CrossRef\]](#)
2. Grigore, M.E.; Holban, A.M.; Grumezescu, A.M. Nanotherapeutics in the management of infections and cancer. In *Nanobiomaterials Science, Development and Evaluation*; Elsevier: Amsterdam, The Netherlands, 2017; pp. 163–189.
3. Amábile-Cuevas, C.F. Global Perspectives of Antibiotic Resistance. In *Antimicrobial Resistance in Developing Countries*; Springer: Berlin/Heidelberg, Germany, 2010; pp. 3–13.
4. Leseva, M.; Arguirova, M.; Nashev, D.; Zamfirova, E.; Hadzhyiski, O. Nosocomial infections in burn patients: Etiology, antimicrobial resistance, means to control. *Ann. Burns Fire Disasters* **2013**, *26*, 5. [\[PubMed\]](#)
5. Corcione, S.; Lupia, T.; De Rosa, F.G. Host and Microbiota Interaction Study Group. M.I.S. Microbiome in the setting of burn patients: Implications for infections and clinical outcomes. *Burns Trauma* **2020**, *8*, 1664–3224. [\[CrossRef\]](#) [\[PubMed\]](#)
6. Bennett, J.V. Nosocomial infections due to *Pseudomonas*. *J. Infect. Dis.* **1974**, *130*, S4–S7. [\[CrossRef\]](#)
7. Al-Dahmashi, H.; Al-Obaidi, R.D.; Al-Khafaji, N. *Pseudomonas aeruginosa: Diseases, Biofilm and Antibiotic Resistance*. In *Pseudomonas Aeruginosa-Biofilm Formation, Infections and Treatments*; Intech Open: London, UK, 2020.
8. Neacsu, I.A.; Leau, S.-A.; Marin, S.; Holban, A.M.; Vasile, B.-S.; Nicoara, A.-I.; Ene, V.L.; Bleotu, C.; Albu Kaya, M.G.; Fikai, A. Collagen-Carboxymethylcellulose Biocomposite Wound-Dressings with Antimicrobial Activity. *Materials* **2021**, *14*, 1153. [\[CrossRef\]](#) [\[PubMed\]](#)
9. Weller, C.D.; Team, V.; Sussman, G. First-line interactive wound dressing update: A comprehensive review of the evidence. *Front. Pharmacol.* **2020**, *11*, 155. [\[CrossRef\]](#)
10. Abazari, M.F.; Gholizadeh, S.; Karizi, S.Z.; Birgani, N.H.; Abazari, D.; Paknia, S.; Derakhshankhah, H.; Allahyari, Z.; Amini, S.M.; Hamidi, M. Recent Advances in Cellulose-Based Structures as the Wound-Healing Biomaterials: A Clinically Oriented Review. *Appl. Sci.* **2021**, *11*, 7769. [\[CrossRef\]](#)
11. Grigore, M.E.; Grumezescu, A.M.; Holban, A.M.; Mogoşanu, G.D.; Andronescu, E. Collagen-nanoparticles composites for wound healing and infection control. *Metals* **2017**, *7*, 516. [\[CrossRef\]](#)
12. Nurwito, B.S.; Maulida, H.N. Electrospun fibers as a wound dressing material using combination of cellulose acetate/collagen seeding stem cell. *Asian J. Microbiol. Biotechnol. Environ. Sci.* **2018**, *20*, s43–s47.
13. Ramanathan, G.; Seleenmary Sobhanadhas, L.S.; Sekar Jeyakumar, G.F.; Devi, V.; Sivagnanam, U.T.; Fardim, P. Fabrication of biohybrid cellulose acetate-collagen bilayer matrices as nanofibrous spongy dressing material for wound-healing application. *Biomacromolecules* **2020**, *21*, 2512–2524. [\[CrossRef\]](#)
14. Samadian, H.; Salehi, M.; Farzamfar, S.; Vaez, A.; Ehterami, A.; Sahrpeyma, H.; Goodarzi, A.; Ghorbani, S. In vitro and in vivo evaluation of electrospun cellulose acetate/gelatin/hydroxyapatite nanocomposite mats for wound dressing applications. *Artif. Cells Nanomed. Biotechnol.* **2018**, *46* (Suppl. 1), 964–974. [\[CrossRef\]](#)
15. Naomi, R.; Fauzi, M.B. Cellulose/collagen dressings for diabetic foot ulcer: A review. *Pharmaceutics* **2020**, *12*, 881. [\[CrossRef\]](#) [\[PubMed\]](#)
16. ur Rehman, S.R.; Augustine, R.; Zahid, A.A.; Ahmed, R.; Tariq, M.; Hasan, A. Reduced graphene oxide incorporated GelMA hydrogel promotes angiogenesis for wound healing applications. *Int. J. Nanomed.* **2019**, *14*, 9603. [\[CrossRef\]](#) [\[PubMed\]](#)
17. Barroso, A.; Mestre, H.; Ascenso, A.; Simões, S.; Reis, C. Nanomaterials in wound healing: From material sciences to wound healing applications. *Nano Select* **2020**, *1*, 443–460. [\[CrossRef\]](#)
18. David, M.E.; Ion, R.-M.; Grigorescu, R.M.; Iancu, L.; Holban, A.M.; Nicoara, A.I.; Alexandrescu, E.; Somoghi, R.; Ganciarov, M.; Vasilievici, G. Hybrid Materials Based on Multi-Walled Carbon Nanotubes and Nanoparticles with Antimicrobial Properties. *Nanomaterials* **2021**, *11*, 1415. [\[CrossRef\]](#) [\[PubMed\]](#)
19. Nosrati, H.; Khouy, R.A.; Nosrati, A.; Khodaei, M.; Banitalebi-Dehkordi, M.; Ashrafi-Dehkordi, K.; Sanami, S.; Alizadeh, Z. Nanocomposite scaffolds for accelerating chronic wound healing by enhancing angiogenesis. *J. Nanobiotechnol.* **2021**, *19*, 1–21. [\[CrossRef\]](#)
20. Ravanbakhsh, H.; Bao, G.; Mongeau, L. Carbon nanotubes promote cell migration in hydrogels. *Sci. Rep.* **2020**, *10*, 1–10.
21. Azizi-Lalabadi, M.; Hashemi, H.; Feng, J.; Jafari, S.M. Carbon nanomaterials against pathogens; the antimicrobial activity of carbon nanotubes, graphene/graphene oxide, fullerenes, and their nanocomposites. *Adv. Colloid Interface Sci.* **2020**, *2020*, 102250. [\[CrossRef\]](#)
22. Laganà, P.; Visalli, G.; Facciola, A.; Ciarello, M.P.; Laganà, A.; Iannazzo, D.; Di Pietro, A. Is the Antibacterial Activity of Multi-Walled Carbon Nanotubes (MWCNTs) Related to Antibiotic Resistance? An Assessment in Clinical Isolates. *Int. J. Environ. Res.* **2021**, *18*, 9310. [\[CrossRef\]](#) [\[PubMed\]](#)
23. Vagos, M.R.; Moreira, J.M.; Soares, O.S.; Pereira, M.F.; Mergulhão, F.J. Incorporation of carbon nanotubes in polydimethylsiloxane to control *Escherichia coli* adhesion. *Polym. Compos.* **2019**, *40* (Suppl. 2), E1697–E1704. [\[CrossRef\]](#)
24. Vagos, M.R.; Gomes, M.; Moreira, J.M.; Soares, O.S.; Pereira, M.F.; Mergulhão, F.J. Carbon nanotube/poly (Dimethylsiloxane) composite materials to reduce bacterial adhesion. *Antibiotics* **2020**, *9*, 434. [\[CrossRef\]](#) [\[PubMed\]](#)
25. Narayan, R.J.; Berry, C.J.; Brigmon, R.L. Structural and biological properties of carbon nanotube composite films. *Mater. Sci. Eng. B* **2005**, *123*, 123–129. [\[CrossRef\]](#)

26. Kittana, N.; Assali, M.; Abu-Rass, H.; Lutz, S.; Hindawi, R.; Ghannam, L.; Zakarneh, M.; Mousa, A. Enhancement of wound healing by single-wall/multi-wall carbon nanotubes complexed with chitosan. *Int. J. Nanomed.* **2018**, *13*, 7195. [[CrossRef](#)] [[PubMed](#)]
27. Pormohammad, A.; Monych, N.K.; Ghosh, S.; Turner, D.L.; Turner, R.J. Nanomaterials in Wound Healing and Infection Control. *Antibiotics* **2021**, *10*, 473. [[CrossRef](#)] [[PubMed](#)]
28. MacDonald, R.A.; Voge, C.M.; Kariolis, M.; Stegemann, J.P. Carbon nanotubes increase the electrical conductivity of fibroblast-seeded collagen hydrogels. *Acta Biomater.* **2008**, *4*, 1583–1592. [[CrossRef](#)]
29. Murugesan, B.; Pandiyan, N.; Kasinathan, K.; Rajaiyah, A.; Arumuga, M.; Subramanian, P.; Sonamuthue, J.; Samayananf, S.; Ravi, V.; Marimuthub, A.; et al. Fabrication of heteroatom doped NFP-MWCNT and NFB-MWCNT nanocomposite from imidazolium ionic liquid functionalized MWCNT for antibiofilm and wound healing in Wistar rats: Synthesis, characterization, in-vitro and in-vivo studies. *Mater. Sci. Eng. C* **2020**, *111*, 110791. [[CrossRef](#)]
30. Das, B.; Chattopadhyay, P.; Upadhyay, A.; Gupta, K.; Mandal, M.; Karak, N. Biophysico-chemical interfacial attributes of Fe<sub>3</sub>O<sub>4</sub> decorated MWCNT nanohybrid/bio-based hyperbranched polyurethane nanocomposite: An antibacterial wound healing material with controlled drug release potential. *New J. Chem.* **2014**, *38*, 4300–4311. [[CrossRef](#)]
31. David, M.E.; Grigorescu, R.M.; Iancu, L.; Andrei, E.R.; Somoghi, R.; Frone, A.N.; Atkinson, I.; Predoana, L.; Nicoara, A.-I.; Ion, R.-M. Synthesis and characterization of multi-walled carbon nanotubes decorated with hydroxyapatite. *Fuller. Nanotub.* **2021**, *29*, 423–430. [[CrossRef](#)]
32. Kokubo, T.; Takadama, H. How useful is SBF in predicting in vivo bone bioactivity? *Biomaterials* **2006**, *27*, 2907–2915. [[CrossRef](#)]
33. Naddafan, M.; Shaker Alattar, A.; Dehghani, Z.; Malekfar, R. Detecting compressive strain by evaluation of Raman spectroscopy of the multiwall Carbon nanotubes/TiO<sub>2</sub> nanocomposites. *Int. J. Nano Dimens.* **2020**, *11*, 168–176.
34. Xie, Y.; Qian, H.; Zhong, Y.; Guo, H.; Hu, Y. Facile low-temperature synthesis of carbon nanotube/nanohybrids with enhanced visible-light-driven photocatalytic activity. *Int. J. Photoenergy* **2012**, *2012*, 682138. [[CrossRef](#)]
35. Wongaree, M.; Chiarakorn, S.; Chuangchote, S. Photocatalytic improvement under visible light in nanoparticles by carbon nanotube incorporation. *J. Nanomater.* **2015**, *2015*, 689306. [[CrossRef](#)]
36. Chan, K.F.; Zaid, M.H.M.; Liza, S.; Matori, K.A.; Mamat, M.S.; Hazan, M.A.; Yaakob, Y. Effect of CNT on microstructural properties of Zn<sub>2</sub>SiO<sub>4</sub>/CNT composite via dry powder processing. *Mater. Res. Express* **2020**, *7*, 105601. [[CrossRef](#)]
37. Gopi, S.; Pius, A.; Kargl, R.; Kleinschek, K.S.; Thomas, S. Fabrication of cellulose acetate/chitosan blend films as efficient adsorbent for anionic water pollutants. *Polym. Bull.* **2019**, *76*, 1557–1571. [[CrossRef](#)]
38. Atieh, M.A.; Bakather, O.Y.; Al-Tawbini, B.; Bukhari, A.A.; Abuilaiwi, F.A.; Fettouhi, M.B. Effect of carboxylic functional group functionalized on carbon nanotubes surface on the removal of lead from water. *Bioinorg. Chem. Appl.* **2010**, *2010*, 603978. [[CrossRef](#)]
39. Kochkina, N.E.; Butikova, O.A. Effect of fibrous TiO<sub>2</sub> filler on the structural, mechanical, barrier and optical characteristics of biodegradable maize starch/PVA composite films. *Int. J. Biol.* **2019**, *139*, 431–439. [[CrossRef](#)] [[PubMed](#)]
40. Arakha, M.; Saleem, M.; Mallick, B.C.; Jha, S. The effects of interfacial potential on antimicrobial propensity of ZnO nanoparticle. *Sci. Rep.* **2015**, *5*, 1–10. [[CrossRef](#)] [[PubMed](#)]
41. Khashan, K.S.; Sulaiman, G.M.; Abdulameer, F.A.; Albukhaty, S.; Ibrahim, M.A.; Al-Muhimeed, T.; AlObaid, A.A. Antibacterial Activity of TiO<sub>2</sub> Nanoparticles Prepared by One-Step Laser Ablation in Liquid. *Appl. Sci.* **2021**, *11*, 4623. [[CrossRef](#)]
42. Xing, Y.; Li, X.; Guo, X.; Li, W.; Chen, J.; Liu, Q.; Xu, Q.; Wang, Q.; Yang, H.; Shui, Y. Effects of different TiO<sub>2</sub> nanoparticles concentrations on the physical and antibacterial activities of chitosan-based coating film. *Nanomaterials* **2020**, *10*, 1365. [[CrossRef](#)]
43. Zare-Zardini, H.; Shanbedi, M.; Soltaninejad, H.; Mohammadzadeh, M.; Amiri, A.; Hamidieh, A.A.; Ferdowsian, F.; Alemi, A.; Hoseinkhani, S.; Fesahat, F. The Effect of Temperature and Acidity on Antimicrobial Activities of Pristine MWCNTs and MWCNTs-Arg. *J. Nanosci. Nanotechnol.* **2020**, *16*, 127–136.
44. Chłopek, J.; Czajkowska, B.; Szaraniec, B.; Frackowiak, E.; Szostak, K.; Beguin, F. In vitro studies of carbon nanotubes biocompatibility. *Carbon* **2006**, *44*, 1106–1111. [[CrossRef](#)]
45. Singh, S.; Shi, T.; Duffin, R.; Albrecht, C.; van Berlo, D.; Höhr, D.; Fubini, B.; Martra, G.; Fenoglio, I.; Borm, P.J. Endocytosis, oxidative stress and IL-8 expression in human lung epithelial cells upon treatment with fine and ultrafine TiO<sub>2</sub>: Role of the specific surface area and of surface methylation of the particles. *Toxicol. Appl. Pharmacol.* **2007**, *222*, 141–151. [[CrossRef](#)] [[PubMed](#)]
46. Thibodeau, M.; Giardina, C.; Hubbard, A. Silica-induced caspase activation in mouse alveolar macrophages is dependent upon mitochondrial integrity and aspartic proteolysis. *Toxicol. Sci.* **2003**, *76*, 91–101. [[CrossRef](#)] [[PubMed](#)]